Generation and eight-port homodyne characterization of time-bin qubits for continuous-variable quantum information processing

Shuntaro Takeda,* Takahiro Mizuta, Maria Fuwa, Jun-ichi Yoshikawa, Hidehiro Yonezawa, and Akira Furusawa†
Department of Applied Physics, School of Engineering, The University of Tokyo, 7-3-1 Hongo, Bunkyo-ku, Tokyo 113-8656, Japan
(Received 23 May 2012; published 3 April 2013)

We experimentally generate arbitrary time-bin qubits using continuous-wave light. The advantage unique to our qubit is its compatibility with deterministic continuous-variable quantum information processing. This compatibility comes from its well-defined spatiotemporal mode and frequency spectrum within the operational bandwidth of the current continuous-variable technology. We also demonstrate an efficient scheme to characterize time-bin qubits via eight-port homodyne measurement. This enables the complete characterization of the qubits as two-mode states, as well as a flexible analysis equivalent to the conventional scheme based on a Mach-Zehnder interferometer and photon detection.

DOI: 10.1103/PhysRevA.87.043803 PACS number(s): 42.50.Dv, 03.65.Wj, 03.67.Bg, 42.50.Ex

There are two complementary approaches in optical quantum information processing: discrete variables (DVs) and continuous variables (CVs). DV experiments are conducted by qubits represented by single-photon optical pulses [1–6]. However, due to inefficient generation and imperfect detection of qubits, most of the experiments are probabilistic and require postselection [7,8]. In contrast, CV experiments rely on the wave nature of light. They can be performed deterministically via quadrature squeezing, highly efficient homodyne detection and feed-forward operations, but their operation fidelities are relatively low due to the limited level of squeezing [9,10]. The difficulty of error correction might be another disadvantage of CV quantum information processing [11]. Recently, there has emerged a "hybrid" approach to combine both techniques to circumvent the current limitations [12]. Its major advantage is deterministic operation of qubits with CV techniques; one of the most striking examples is deterministic quantum teleportation of qubits with a CV teleporter, as is proposed in Refs. [13,14]. The recent experiment on CV teleportation of highly nonclassical optical pulses [15] opens the way to this hybrid teleportation. This CV teleporter is based on continuous waves; however, typical qubits are generated by pulse-pumped spontaneous parametric downconversion (SPDC) [1–6]. The bandwidth of these qubits is orders of magnitude wider than the operational bandwidth of the CV teleporter (only around 10 MHz).

Here we overcome this incompatibility by generating a time-bin qubit using cw light. This qubit consists of two temporally separated optical pulses, described as a superposition of a photon in one pulse $|1,0\rangle$ and the other pulse $|0,1\rangle$: $|\psi\rangle = c_0|1,0\rangle + c_1 e^{i\Phi}|0,1\rangle$. Thus far, such qubits have been prepared by pulsed lasers [3–5] and used as a key resource for various DV experiments over long distances (e.g., quantum cryptography [16,17], quantum teleportation [18], and entanglement swapping [19]). In contrast, our time-bin qubit is generated from a cw-pumped, nondegenerate optical parametric oscillator (NOPO), which is a cavity-enhanced version of the SPDC. The NOPO cavity enhances the SPDC process only inside its resonant mode, thereby generating qubits in a well-defined and controlled spatiotemporal mode. The 6.2-MHz bandwidth of the resultant qubit is within the bandwidth of the squeezing and homodyne-based feed-forward operations (currently up to tens of megahertz), which mainly limits the bandwidth of the CV teleporter in Ref. [15]. Thus our qubit is fully compatible with the teleporter as well as more advanced CV experiments based on such techniques. Another advantage is that our qubits can be readily teleported by a single CV teleporter (such as Ref. [15]), since the two pulses have the same polarization, while polarization qubits require two CV teleporters (one for each polarization) [14]. Such high compatibility should open the way for further hybrid protocols.

For the characterization of time-bin qubits, we develop a scheme via eight-port homodyne measurement [20–22]. Unlike the other schemes based on photon detection [3] or regular homodyne measurement [5,6], our scheme provides a simple and efficient way to independently measure two pulses without varying any optical phase of the system. This enables the reconstruction of the complete two-mode density matrices, not only in the qubit subspace spanned by $\{|1,0\rangle,|0,1\rangle\}$, but in a much wider photon-number space, including vacuum and multiphoton components. Additionally, we show that the analysis equivalent to the conventional photon-detection scheme [3] can be performed more flexibly for various detection conditions with the same setting.

Our scheme [Fig. 1(a)] is based on the setup for generating single photons in Ref. [23]. In this setup, an NOPO is weakly pumped to produce correlated photon pairs in signal and idler modes written as [24,25]

$$\int dt dt' C(t-t')\hat{a}_{\rm s}^{\dagger}(t)\hat{a}_{\rm i}^{\dagger}(t')\,|0\rangle_{\rm s}\,|0\rangle_{\rm i}\,. \tag{1}$$

Here, $\hat{a}_{\rm s}^{\dagger}(t)$ and $\hat{a}_{\rm i}^{\dagger}(t)$ are creation operators in the signal and idler mode, respectively, and $C(t-t')$ denotes the correlation function between these two modes. A photon-detection event in the idler mode at time $t=0$ projects this state onto $\hat{a}_{\rm i}^{\dagger}(t=0)\,|0\rangle_{\rm i}$. It produces a single-photon state $\hat{A}_{\rm s}^{\dagger}\,|0\rangle_{\rm s}$, where $\hat{A}_{\rm s}^{\dagger} = \int dt C(t)\hat{a}_{\rm s}^{\dagger}(t)/N$ and $N = (\int dt\,|C(t)|^2)^{1/2}$. The temporal mode of this photon is defined by the mode function $f(t) = C(t)/N$, which converges to $f_0(t) = \sqrt{\gamma}e^{-\gamma|t|}$ in the weak pumping limit (γ: NOPO bandwidth) [26].

*takeda@alice.t.u-tokyo.ac.jp
†akiraf@ap.t.u-tokyo.ac.jp

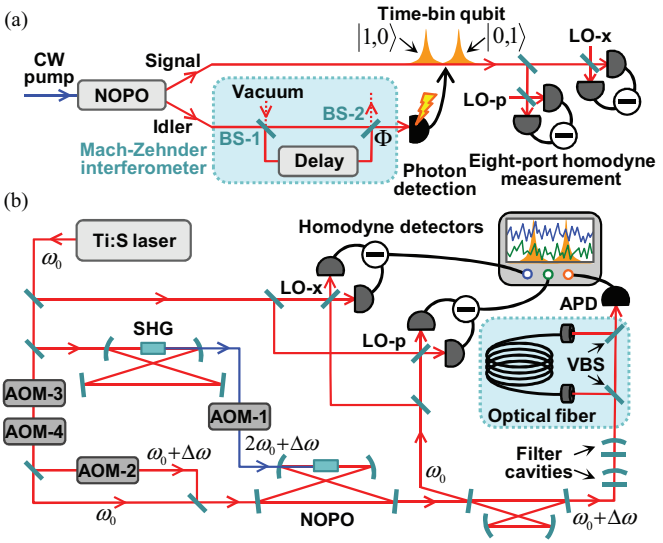

FIG. 1. (Color online) (a) Schematic. (b) Experimental setup. AOM, acousto-optic modulator; APD, avalanche photodiode; BS, beam splitter; cw, continuous wave; LO, local oscillator; NOPO, nondegenerate optical parametric oscillator; SHG, second harmonic generation; and VBS, variable beam splitter.

To obtain time-bin qubits, we introduce an unbalanced Mach-Zehnder interferometer (MZI) into the idler channel as in Ref. [5]. This MZI manipulates the time correlation between the signal and idler modes before photon detection, thereby reshaping the temporal mode in which photons are generated. This scheme originates from the theoretical proposal in Ref. [27] and the subsequent experiments in Refs. [28–30], in which an unbalanced MZI is introduced to violate Bell's inequality by generating energy-time entanglement. We use this entanglement as a resource of time-bin qubits by detecting one of the entangled modes (the idler mode). This MZI reduces the generation rate by discarding one of the two output ports (it can be avoided in theory as mentioned below) but does not degrade the purity of the generated qubits.

To model this scheme, we first introduce an auxiliary vacuum mode "v" and define the beam-splitter (BS) operation on mode "i" and "v" as replacements of $\hat{a}_i^\dagger(t) \to \tau\hat{a}_i^\dagger(t) - \rho e^{-i\Phi}\hat{a}_v^\dagger(t)$ and $\hat{a}_v^\dagger(t) \to \rho e^{i\Phi}\hat{a}_i^\dagger(t) + \tau\hat{a}_v^\dagger(t)$, where τ, ρ, and Φ are the amplitude transmissivity, reflectivity, and relative phase, respectively ($\tau^2+\rho^2=1$). BS-1 ($\tau_1, \rho_1, \Phi_1 = 0$) transforms Eq. (1) into

$$\int dtdt'[\tau_1 C(t-t')\hat{a}_s^\dagger(t)\hat{a}_i^\dagger(t') - \rho_1 C(t-t')\hat{a}_s^\dagger(t)\hat{a}_v^\dagger(t')] \times |0\rangle_s |0\rangle_i |0\rangle_v . \quad (2)$$

By introducing a time delay Δt in mode "v", the $C(t-t')$ on $\hat{a}_s^\dagger(t)\hat{a}_v^\dagger(t')$ is replaced by $C(t-(t'-\Delta t))$. Mode "i" and "v" are then recombined by BS-2 with (τ_2, ρ_2, Φ_2). After this operation, the only term relevant to the photon detection on mode "i" has the form

$$\int dtdt'[\tau_1\tau_2 C(t-t') - \rho_1\rho_2 e^{i\Phi_2} C(t-t'+\Delta t)] \times \hat{a}_s^\dagger(t)\hat{a}_i^\dagger(t')|0\rangle_s |0\rangle_i |0\rangle_v . \quad (3)$$

By projecting this state onto $\hat{a}_i^\dagger(t=0)|0\rangle_i$ and tracing out the unused mode "v", we obtain

$$\int dt[\tau_1\tau_2 C(t) - \rho_1\rho_2 e^{i\Phi_2} C(t+\Delta t)]\hat{a}_s^\dagger(t)|0\rangle_s . \quad (4)$$

When Δt is sufficiently long compared to the photon coherence time ($\sim 1/\gamma$) between the signal and idler modes, the two modes defined by $\hat{A}_1^\dagger = \int dt C(t)\hat{a}_s^\dagger(t)/N$ and $\hat{A}_2^\dagger = \int dt C(t+\Delta t)\hat{a}_s^\dagger(t)/N$ can be regarded as orthogonal. Thus, from Eq. (4), the two-mode state can be described as $|\psi\rangle_{12} \propto \tau_1\tau_2|1\rangle_1|0\rangle_2 - \rho_1\rho_2 e^{i\Phi_2}|0\rangle_1|1\rangle_2$. The delay ($t' \to t' - \Delta t$) in the idler mode induces an earlier time bin ($t \to t + \Delta t$) in the signal mode, and the two time bins constitute a single time-bin qubit. The coefficients of the qubit are determined by the splitting ratio of both BS-1 and BS-2, as well as the recombining phase at BS-2; we experimentally show that they are arbitrarily tunable. In the weak pumping regime, the mode function of each time bin is written as $f_1(t) = \sqrt{\gamma}e^{-\gamma|t|}$ and $f_2(t) = \sqrt{\gamma}e^{-\gamma|t+\Delta t|}$. Note that when the photon detection is performed on the other output port of BS-2 instead, $|\psi'\rangle_{12} \propto \tau_1\rho_2|1\rangle_1|0\rangle_2 + \rho_1\tau_2 e^{i\Phi_2}|0\rangle_1|1\rangle_2$ is obtained. By adding photon-detection events of this port and performing an appropriate unitary transformation thereafter, the MZI-induced reduction of the generation rate is avoidable, though not experimentally shown here.

Our detailed experimental setup is shown in Fig. 1(b). Part of the output beam of the Ti:sapphire laser (wavelength 860 nm) is frequency doubled by a second-harmonic generation cavity (frequency: $\omega_0 \to 2\omega_0$). Its frequency is then shifted with an acousto-optic modulator (AOM-1) by 590 MHz ($2\omega_0 \to 2\omega_0 + \Delta\omega$), which corresponds to the free spectrum range (FSR) of our NOPO. 10 mW of this beam pumps the NOPO [half-width at half maximum (HWHM) 6.2 MHz ($=\gamma/2\pi$)], producing signal (ω_0) and idler ($\omega_0 + \Delta\omega$) photons. Two weak coherent beams ($\omega_0, \omega_0 + \Delta\omega$) are also injected into the NOPO to lock the subsequent system. Both beams are alternatively blocked and unblocked by AOM-3 and 4 at a rate of 2 kHz. The signal and idler modes are spatially separated by a cavity (HWHM 22.2 MHz, FSR

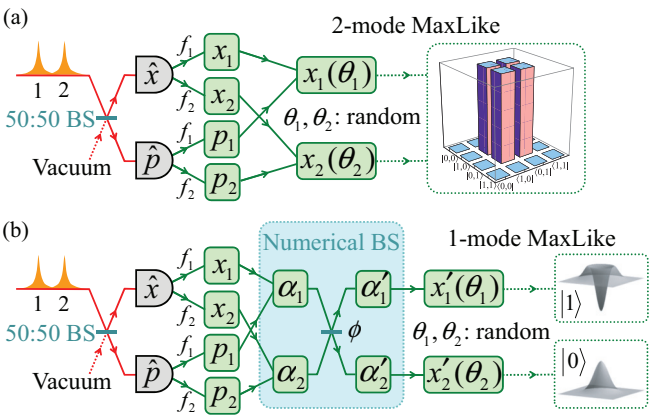

FIG. 2. (Color online) Eight-port homodyne analysis of time-bin qubits. BS, beam splitter; and MaxLike, maximum likelihood algorithm. (a) Reconstruction of two-mode density matrices. (b) The analysis equivalent to the conventional photon-detection scheme.

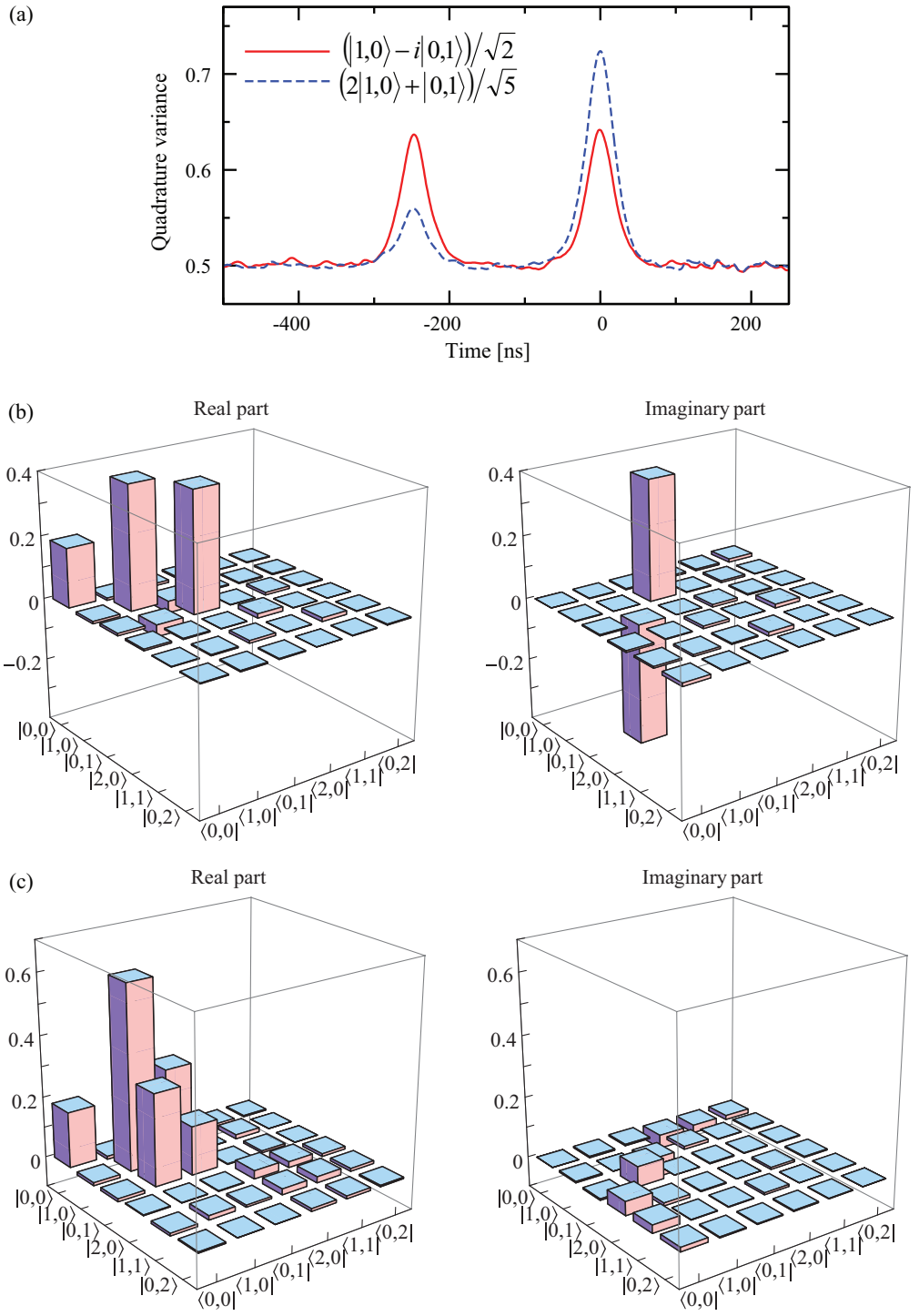

FIG. 3. (Color online) Experimental results. Quadrature variance at each time point (a) (vacuum variance is normalized to 1/2) and density matrices of (b) $(|1,0\rangle - i|0,1\rangle)/\sqrt{2}$ and (c) $(2|1,0\rangle + |0,1\rangle)/\sqrt{5}$.

1150 MHz). The idler mode is then injected into a MZI after filtering out irrelevant NOPO modes via two filter cavities. In the MZI, part of the idler mode is split off by a variable BS (VBS), composed of a half wave plate and a polarizing BS. The split-off part is transmitted through a 50-m optical fiber (PM780-HP, Thorlabs), and is then recombined with another VBS. Here the delay is set to $\Delta t = 242$ ns so that the overlap between two time bins is negligible [$\int f_1(t) f_2(t) dt \sim 0.08\%$]. The optical path length difference is passively stabilized by surrounding the fiber with heat-insulating material, as well as actively locked to a target value with piezoactuators. One output port of the MZI is sent to an avalanche photodiode (APD) to herald time-bin qubits, whereas the other is monitored by a photodetector to phase lock the MZI.

In general, complete homodyne characterization of two-mode states requires two-mode quadrature measurements at

various phase sets (θ_1,θ_2) [6]. One possible way to carry out this in our case is to spatially separate two time bins and then perform a homodyne measurement on each bin with careful control of the local oscillator's phase. However, since two bins have the same polarization and are temporally close to each other, such a separation requires high-speed switching with high precision. In Ref. [5], only the relative phase of two time bins are scanned instead of fully scanning the local oscillators' phases, but this scheme is inapplicable when characterizing unknown qubit states. Here, we propose a more efficient scheme via eight-port homodyne measurement [20–22], where no optical phase scanning is required. First, both time bins are split with a 50:50 BS for two homodyne measurements for orthogonal quadratures $\hat{x}$ and $\hat{p}$. By multiplying $f_1(t)$ and $f_2(t)$ to each homodyne photocurrent, we can obtain the quadratures (x_1,p_1,x_2,p_2) with extra vacuum noise from the unused port of the BS [Fig. 2(a)]; this vacuum noise is the inevitable consequence of the simultaneous measurement of conjugate variables $\hat{x}$ and $\hat{p}$ [31]. From this set, quadratures at any phase θ can be calculated as $x_j(\theta) = x_j\cos\theta + p_j\sin\theta$ $(j = 1,2)$. Therefore, from one set, we can randomly select a phase set (θ_1,θ_2) and construct two independent tomography data sets $(x_1(\theta_1),x_2(\theta_2))$ and $(x_1(\theta_1+\pi/2),x_2(\theta_2+\pi/2))$ which refer to orthogonal quadratures. In the experiment, 100 000 quadrature sets are acquired and 200 000 tomography data sets are constructed. The maximum likelihood algorithm [32] is then used to reconstruct two-mode density matrices in the Fock basis: $\hat{\rho} = \sum_{k,l,m,n=0}^{\infty} \rho_{klmn}\,|k,l\rangle\langle m,n|$. Here we compensate only the extra vacuum noise added in the dual-homodyne measurement, and not other experimental imperfections. The scheme mentioned above can be easily extended to single- or higher-mode states, which shows that eight-port homodyne measurement is a useful tool for characterizing multimode states. Note that in the present setting, the eight-port homodyne measurement is directly measuring the two-mode Q function of a qubit [33,34]. Once the Q function is estimated from the collected data, the corresponding density matrix can be calculated in theory [35]. Instead, we have mapped the measured data (x_1,p_1,x_2,p_2) to $(\theta_1,x_1(\theta_1),\theta_2,x_2(\theta_2))$, from which we can directly calculate the density matrix using the standard maximum likelihood algorithm [32].

We generated eight types of qubits: $(|1,0\rangle + e^{i\Phi}|0,1\rangle)/\sqrt{2}$ and $(2|1,0\rangle + e^{i\Phi}|0,1\rangle)/\sqrt{5}$ with $\Phi = 0,\pi,\pm\pi/2$. Figure 3(a) shows the quadrature variance at each time point calculated from the 100 000 quadrature traces, where the vacuum variance is normalized to 1/2 ($\hbar = 1$). Two time bins appear as the two peaks of the trace, and the peak height above the vacuum noise level corresponds to the probability of existing photons [23]. Experimental density matrices in Figs. 3(b) and 3(c) show not only the qubit submatrix spanned by $\{|1,0\rangle, |0,1\rangle\}$, but also the vacuum and multiphoton contributions. Ideally, generated states have components only in the qubit submatrix. In practice, the density matrices show $18\% \pm 1\%$ of a vacuum (ρ_{0000}), $77\% \pm 1\%$ of a qubit ($\rho_{1010} + \rho_{0101}$), and $5\% \pm 1\%$ of multiphoton components ($1 - \rho_{0000} - \rho_{1010} - \rho_{0101}$). The ratio of diagonal elements ρ_{1010} to ρ_{0101} is equal to the ratio of $|1,0\rangle$ to $|0,1\rangle$, whereas the off-diagonal elements ρ_{1001} and ρ_{0110} demonstrate the superposition of $|1,0\rangle$ and $|0,1\rangle$ at the target phase. The encoded quantum information can be read out by extracting and renormalizing the qubit submatrix. The average fidelity of each submatrix with its target state is 0.989 ± 0.004, showing the highly precise qubit preparation.

The 18% vacuum contribution is well explained by the estimated loss of $1 - \eta_{\rm all} = 16\%$, where $\eta_{\rm all} = \eta_{\rm NOPO}\eta_{\rm vis}^2\eta_{\rm pr}\eta_{\rm det}\eta_{\rm APD}$ is the overall efficiency. Here $\eta_{\rm NOPO} = 0.98$ is the escape efficiency of the NOPO, $\eta_{\rm vis} = 0.98$ the average mode-matching visibility at the eight-port homodyne measurement, $\eta_{\rm pr} = 0.96$ the propagation efficiency from the NOPO to the homodyne detectors, $\eta_{\rm det} = 0.95$ the average detection efficiency given by the quantum efficiency of photodiodes and the electronic noise, and $\eta_{\rm APD} = (\zeta_{\rm tot} - \zeta_{\rm dark})/\zeta_{\rm tot} = 0.98$ the purity of the photon-detection event given by the total count rate $\zeta_{\rm tot} = 5800\ {\rm s}^{-1}$ and the dark count rate $\zeta_{\rm dark} = 80\ {\rm s}^{-1}$.

Our eight-port homodyne setup also enables the analysis equivalent to the conventional detection scheme in Fig. 4(a), where two time bins are recombined via MZI and then the existence of photons at each output mode is monitored by photon detections D_1 and D_2. In this case, D_1 and D_2 correspond to the projection onto orthogonal qubit bases, and if the BS parameters are chosen properly, photons arrive at only one of the two. In our system, this BS can be realized by analytically mixing measured quadratures of two time bins after the measurement [Fig. 2(b)]. For a quadrature data set (x_1,p_1,x_2,p_2), the complex amplitude of each mode can be written as $\alpha_j = (x_j + ip_j)/\sqrt{2}$ $(j = 1,2)$. When the BS recombines these two time bins with (τ',ρ',ϕ), the output amplitude (α_1',α_2') can be calculated as $\alpha_1' = \tau'\alpha_1 + \rho' e^{i\phi}\alpha_2$ and $\alpha_2' = -\rho' e^{-i\phi}\alpha_1 + \tau'\alpha_2$. Finally, the output quadratures at any given phase θ can be calculated from these amplitudes as

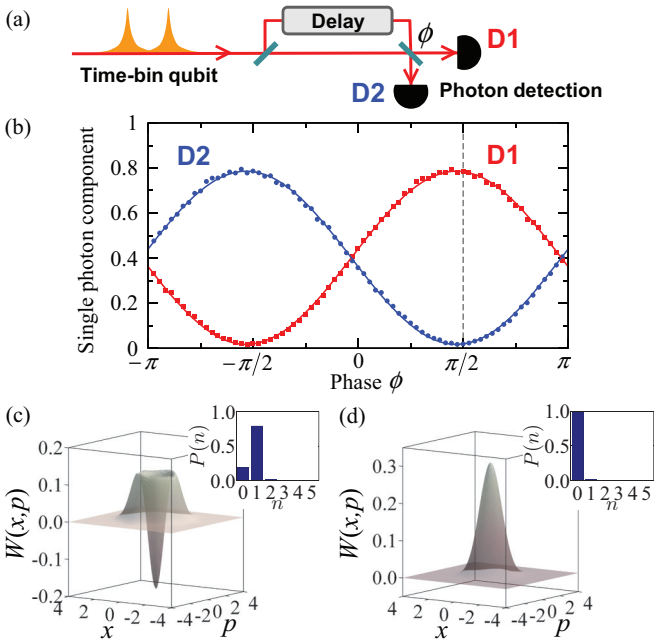

FIG. 4. (Color online) (a) Conventional photon-detection scheme. (b) The ϕ dependence of single-photon components of two modes which are subject to photon detections D_1 and D_2. (c), (d): Experimental Wigner functions $W(x,p)$ and photon-number distributions $P(n)$ at $\phi = \pi/2$.

$x'_j(\theta) = (\alpha'_j e^{-i\theta} + \alpha'^*_j e^{i\theta})/\sqrt{2}$. Therefore we can compose a data set $(x'_1(\theta_1), x'_2(\theta_2))$ for any desired BS parameters (τ', ρ', ϕ) and any phase set (θ_1, θ_2). As a result, the density matrix of each mode subject to D_1 or D_2 can be reconstructed by a maximum likelihood algorithm compensating the extra vacuum noise. In the special case of choosing $(\tau', \rho', \phi) = (c_0, c_1, -\Phi)$ or $(c_1, c_0, -\Phi + \pi)$ for an initial time-bin qubit $|\psi\rangle_{12} = c_0 |1\rangle_1 |0\rangle_2 + c_1 e^{i\Phi} |0\rangle_1 |1\rangle_2$, the two modes would theoretically be decomposed into a single-photon state and a vacuum state. In our eight-port homodyne scheme, the whole set $\{(\tau', \rho', \phi)\}$ of the D_1-D_2 measurement results can be obtained from a single quadrature data set. Some related discussions on this photon-vacuum decomposition were made in terms of the cross section of two-mode Wigner function in Refs. [5,6].

We analyzed the data set of the qubit $|\psi\rangle = (|1,0\rangle - i|0,1\rangle)/\sqrt{2}$ for a fixed $\tau' = \rho' = 1/\sqrt{2}$ and varying ϕ. The ϕ dependence of the single-photon component of D_1 and D_2 [Fig. 4(b)] shows the fringe visibility of $96 \pm 2\%$. It reaches its minimum and maximum around $\pm\pi/2$, demonstrating the generation of the target qubit state. The reconstructed states at $\phi = \pi/2$ are explicitly decomposed into a single photon and a vacuum. Figure 4(c) shows $P_a(1) = 0.79$ of a single-photon component and a strong negativity of the Wigner function $W_a(0,0) = -0.187$. Figure 4(d) is an almost pure vacuum with $P_b(0) = 0.98$. $P_b(1) = 0.02$ of a photon still remains, possibly because the BS parameters (τ', ρ', ϕ) are not optimal and the phase Φ of the qubit fluctuated during the measurement.

In summary, we have generated arbitrary time-bin qubits in a well-defined spatiotemporal mode by using a cw-pumped NOPO. The generated qubit is compatible with the current CV operations, thereby providing an essential tool for hybrid approaches in quantum information processing. Our eight-port homodyne scheme efficiently reconstructed the full two-mode density matrices of the qubits, and also enabled the analysis equivalent to the conventional photon-detection scheme by a numerical BS operation. This characterization scheme is universal and applicable to single- or multimode states encoded in different temporal modes [3–5], spatial modes [2,6], or polarization modes [1].

This work was partly supported by the SCOPE program of the MIC of Japan, PDIS, GIA, G-COE, APSA, and FIRST commissioned by the MEXT of Japan, and ASCR-JSPS.

[1] P. G. Kwiat, K. Mattle, H. Weinfurter, A. Zeilinger, A. V. Sergienko, and Y. Shih, Phys. Rev. Lett. **75**, 4337 (1995).
[2] J. G. Rarity and P. R. Tapster, Phys. Rev. Lett. **64**, 2495 (1990).
[3] J. Brendel, N. Gisin, W. Tittel, and H. Zbinden, Phys. Rev. Lett. **82**, 2594 (1999).
[4] I. Marcikic, H. de Riedmatten, W. Tittel, V. Scarani, H. Zbinden, and N. Gisin, Phys. Rev. A **66**, 062308 (2002).
[5] A. Zavatta, M. D'Angelo, V. Parigi, and M. Bellini, Phys. Rev. Lett. **96**, 020502 (2006).
[6] S. A. Babichev, J. Appel, and A. I. Lvovsky, Phys. Rev. Lett. **92**, 193601 (2004).
[7] W. Tittel and G. Weihs, Quantum Inf. Comput. **1**, 3 (2001).
[8] J.-W. Pan, Z.-B. Chen, C.-Y. Lu, H. Weinfurter, A. Zeilinger, and M. Żukowski, Rev. Mod. Phys. **84**, 777 (2012).
[9] A. Furusawa, J. K. Sørensen, S. L. Braunstein, C. A. Fuchs, H. J. Kimble, and E. S. Polzik, Science **282**, 706 (1998).
[10] J. Yoshikawa, T. Hayashi, T. Akiyama, N. Takei, A. Huck, U. L. Andersen, and A. Furusawa, Phys. Rev. A **76**, 060301(R) (2007).
[11] J. Niset, J. Fiurášek, and N. J. Cerf, Phys. Rev. Lett. **102**, 120501 (2009).
[12] A. Furusawa and P. van Loock, *Quantum Teleportation and Entanglement: A Hybrid Approach to Optical Quantum Information Processing* (Wiley, New York, 2011).
[13] T. Ide, H. F. Hofmann, T. Kobayashi, and A. Furusawa, Phys. Rev. A **65**, 012313 (2001).
[14] A. Dolínska, B. C. Buchler, W. P. Bowen, T. C. Ralph, and P. K. Lam, Phys. Rev. A **68**, 052308 (2003).
[15] N. Lee, H. Benichi, Y. Takeno, S. Takeda, J. Webb, E. Huntington, and A. Furusawa, Science **332**, 330 (2011).
[16] R. J. Hughes, G. L. Morgan, and C. G. Peterson, J. Mod. Opt. **47**, 533 (2000).
[17] I. Marcikic, H. de Riedmatten, W. Tittel, H. Zbinden, M. Legré, and N. Gisin, Phys. Rev. Lett. **93**, 180502 (2004).
[18] I. Marcikic, H. de Reidmatten, W. Tittel, H. Zbinden, and N. Gisin, Nature (London) **421**, 509 (2003).
[19] H. de Riedmatten, I. Marcikic, J. A. W. van Houwelingen, W. Tittel, H. Zbinden, and N. Gisin, Phys. Rev. A **71**, 050302(R) (2005).
[20] N. G. Walker and J. E. Carroll, Electon. Lett. **20**, 981 (1984).
[21] N. G. Walker and J. E. Carroll, Opt. Quantum Electron. **18**, 355 (1986).
[22] N. G. Walker, J. Mod. Opt. **34**, 15 (1987).
[23] J. S. Neergaard-Nielsen, B. M. Nielsen, H. Takahashi, A. I. Vistnes, and E. S. Polzik, Opt. Express **15**, 7491 (2007).
[24] R. Loudon, *The Quantum Theory of Light*, 3rd ed. (Oxford Science Publications, Oxford, 2000).
[25] S. Takeda, H. Benichi, T. Mizuta, N. Lee, J. Yoshikawa, and A. Furusawa, Phys. Rev. A **85**, 053824 (2012).
[26] K. Mølmer, Phys. Rev. A **73**, 063804 (2006).
[27] J. D. Franson, Phys. Rev. Lett. **62**, 2205 (1989).
[28] J. Brendel, E. Mohler, and W. Martienssen, Europhys. Lett. **20**, 575 (1992).
[29] P. G. Kwiat, A. M. Steinberg, and R. Y. Chiao, Phys. Rev. A **47**, R2472 (1993).
[30] W. Tittel, J. Brendel, H. Zbinden, and N. Gisin, Phys. Rev. Lett. **81**, 3563 (1998).
[31] E. Arthurs and J. L. Kelly, Jr., Bell Syst. Tech. J. **44**, 725 (1965).
[32] A. I. Lvovsky, J. Opt. B: Quantum Semiclassical Opt. **6**, S556 (2004).
[33] M. Freyberger and W. Schleich, Phys. Rev. A **47**, R30 (1993).
[34] U. Leonhardt and H. Paul, Phys. Rev. A **47**, R2460 (1993).
[35] U. Leonhardt, *Essential Quantum Optics: From Quantum Measurement to Black Holes* (Cambridge University Press, Cambridge, UK, 2010).